PHYSICAL REVIEW B **86**, 140102(R) (2012)

Interface dipole between two metallic oxides caused by localized oxygen vacancies

Albina Y. Borisevich,[1,*] Andrew R. Lupini,[1] Jun He,[1,2] Eugene A. Eliseev,[3] Anna N. Morozovska,[4] George S. Svechnikov,[4] Pu Yu,[5] Ying-Hao Chu,[6] Ramamoorthy Ramesh,[5] Sokrates T. Pantelides,[2,1] Sergei V. Kalinin,[1] and Stephen J. Pennycook[1,2]

[1]*Oak Ridge National Laboratory, Oak Ridge, Tennessee 37831, USA*

[2]*Department of Physics and Astronomy, Vanderbilt University, Nashville, Tennessee, USA*

[3]*Institute for Problems of Materials Science, National Academy of Science of Ukraine, 3, Krjijanovskogo, 03142 Kiev, Ukraine*

[4]*Institute of Semiconductor Physics, National Academy of Science of Ukraine, 41, pr. Nauki, 03028 Kiev, Ukraine*

[5]*Department of Materials Science and Engineering and Department of Physics, University of California, Berkeley, California, 94720, USA*

[6]*Department of Materials Science and Engineering, National Chiao Tung University, Hsinchu, Taiwan 30013, Republic of China*

(Received 31 October 2011; revised manuscript received 15 May 2012; published 11 October 2012)

Oxygen vacancies are increasingly recognized to play a role in phenomena observed at transition-metal oxide interfaces. Here, we report a study of $SrRuO_3$ and $La_{0.7}Sr_{0.3}MnO_3$ interfaces using a combination of quantitative aberration-corrected scanning transmission electron microscopy, electron energy-loss spectroscopy, and density functional calculations. Cation displacements are observed at the interface, indicative of a dipolelike electric field even though both materials are nominally metallic. The observed displacements are reproduced by theory if O vacancies are present in the near-interface $La_{0.7}Sr_{0.3}MnO_3$ layers. The results suggest that atomic-scale structural mapping can serve as a quantitative indicator of the presence of O vacancies at interfaces.

DOI: 10.1103/PhysRevB.86.140102 PACS number(s): 68.37.Ma, 61.72.jd, 71.15.Mb

Emergent electronic and structural phenomena at transition-metal oxide (TMO) interfaces have become one of the key areas of condensed matter physics. This interest is driven strongly by applications necessitating development of materials with novel superconducting,[1] transport,[2] and magnetoelectric functionalities.[3] These applications are enabled by a broad spectrum of physical and chemical phenomena due to charge mismatch,[2] polarization discontinuities,[4] orbital ordering,[5] spin reconstruction,[6–10] ionic transfer and vacancy segregation,[11,12] or octahedral tilt effects.[13,14] One of the key aspects of oxide interfaces is the multiple electronic, magnetic, structural, and chemical mechanisms that can be operational at the same time. This variety of effects can greatly complicate the identification of the individual physical phenomena[15] and necessitates comprehensive studies of all aspects of interfacial behavior.[16]

The role of oxygen vacancies in the above phenomena has been largely unexplored. It is well known that many materials such as manganites, cobaltites, and nickelates have large (3–10%) concentrations of oxygen vacancies that strongly depend on oxygen activity. Mitchell *et al*. have demonstrated that relatively small changes in oxygen partial pressure (four orders of magnitude in pO_2 corresponding to ∼25–50 meV in electrochemical potential) can affect the phase diagram of $La_{0.7}Sr_{0.3}MnO_3$ similar to 25% doping.[17] These effects can be expected to be even more pronounced at interfaces with large built-in electric fields. Recent studies by the groups of Skowronski[18] and Cheong[19] have demonstrated that vacancies on the nanoscale can be mobile even at room temperature and hence cannot be assumed to be frozen. This recognition of the role of vacancies is contrasted with the lack of local observations; indeed, only in the cases of well-established vacancy ordering, such as mixed-valence cobaltites[20,21] and high-temperature superconductors[22] can the oxygen vacancies be unequivocally detected. Density functional calculations, however, in conjunction with experimental data can offer strong evidence for their presence or absence.[11]

In this Rapid Communication, we explore the structural and electronic behavior at the interface between the $SrRuO_3$ and $(La_{0.7}Sr_{0.3})MnO_3$ using quantitative aberration-corrected scanning transmission electron microscopy (STEM) and electron energy-loss spectroscopy (EELS), extending the approach suggested for transmission electron microscopy (TEM) by Jia[23–25] that has been recently adapted for STEM.[11,13,26] The cation displacement profile at the nominally metal-metal $SrRuO_3$–$La_{0.7}Sr_{0.3}MnO_3$ interface is visualized directly. The observed displacements can be interpreted as indicative of an interfacial electric dipole. We show that the observed cation displacement pattern can be reproduced quantitatively by density functional theory (DFT) if oxygen vacancies are present at the interface. Furthermore, the electronic potential profiles obtained from DFT and extracted from the STEM data by phenomenological modeling match closely. The implications for the electronic and magnetic properties are discussed.

$La_{0.7}Sr_{0.3}MnO_3$ thin films (with the thickness of 6 nm) were grown on (001) single-crystal $SrTiO_3$ substrate using pulsed laser deposition at 700 °C and an O_2 pressure of 300 mTorr. Subsequently, the $SrRuO_3$ layer (with the thickness of 30 nm) was grown on $La_{0.7}Sr_{0.3}MnO_3$ buffered $SrTiO_3$ at 700 °C and with an O_2 pressure of 100 mTorr. High-angle annular dark-field (HAADF) STEM imaging and EELS studies were carried out using VG Microscopes HB603U operated at 300 kV and equipped with a Nion® aberration corrector and Gatan Enfina® spectrometer.

The HAADF STEM image of the $SrRuO_3$–$La_{0.7}Sr_{0.3}MnO_3$ interface is shown in Fig. 1(a), demonstrating a clear transition between $La_{0.7}Sr_{0.3}MnO_3$ and $SrRuO_3$. In this mode, atomic column intensity is roughly proportional to the square of atomic number Z, so constituent elements can be deduced by tracking column intensities.[27] Analysis of A-site and B-site intensities across the $SrRuO_3$–$La_{0.7}Sr_{0.3}MnO_3$ interface for multiple images shows that at the transition columns with intermediate intensities are often present, on the scale of up

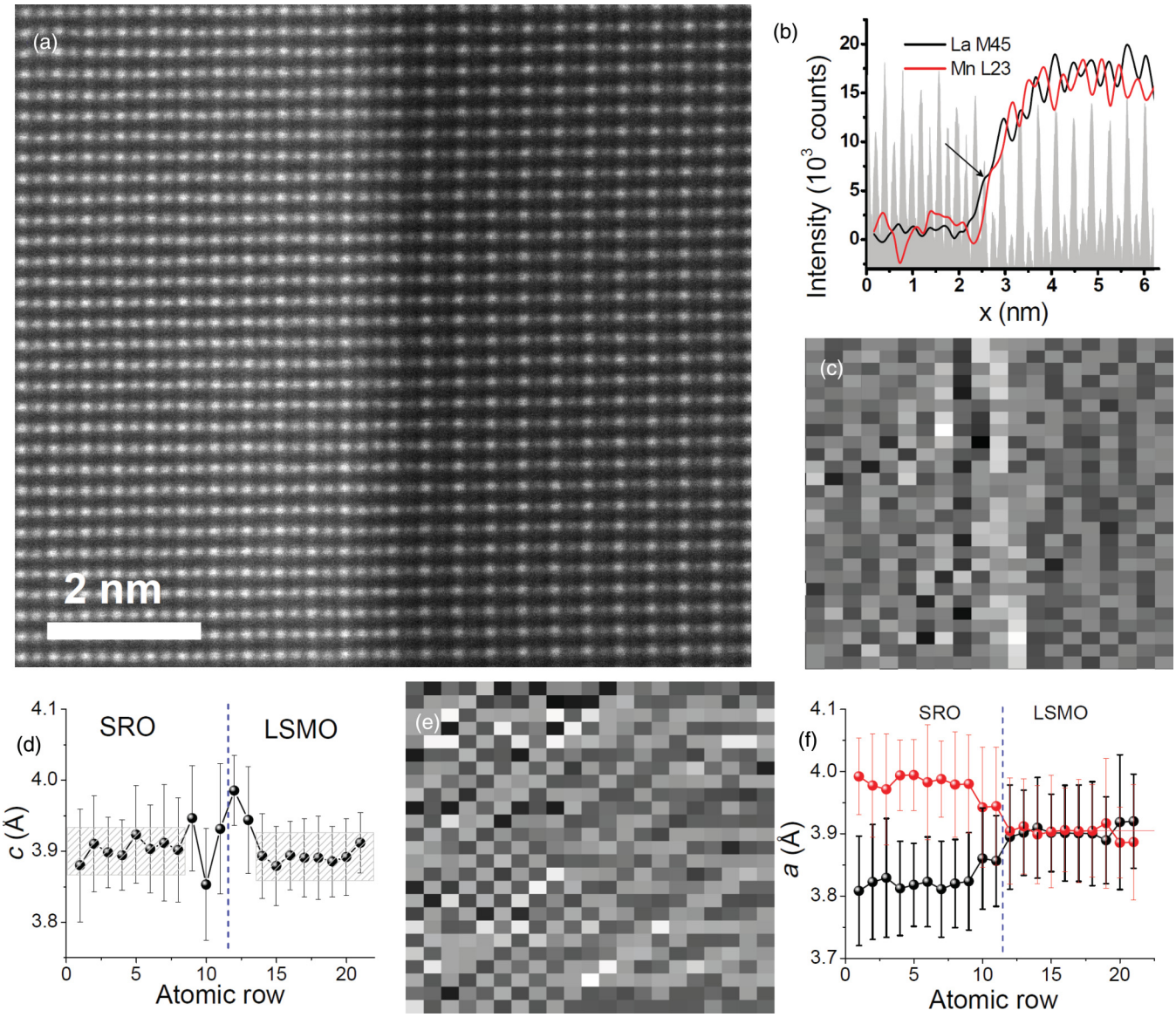

FIG. 1. (Color online) (a) HAADF image of the $SrRuO_3$–$La_{0.7}Sr_{0.3}MnO_3$ interface (b) integrated intensities of La M4,5 and Mn L2,3 edges across the interface illustrating interface sharpness and effective (La,Sr)O-RuO_2 termination; a line profile of the ADF image (background subtracted) is given in light gray for comparison. (c) and (e) Two-dimensional maps of the (c) out-of-plane, or *c* and (e) in-plane, or *a* pseudocubic lattice parameters computed from Fig. 1(a). (d) and (f) Profiles of the maps in (c) and (e) calculated by averaging along the interface. In Fig. 1(d), cross-hatched rectangles cover the points that do not show statistically significant changes (see text). Error bars in profiles (d) and (f) show standard deviation with respect to averaging along the interface in the maps (c) and (e).

to one unit cell for Mn/Ru sublattice and on the scale of 0–2 unit cells for Sr/La sublattice, similar to that observed by Ziese *et al.*[28] in $SrRuO_3$–$La_{0.7}Sr_{0.3}MnO_3$ multilayers. Along the interface the films appear uniform, with no evidence of the extended defects reported to arise in nonoptimal growth conditions.[29] The number of intermediate intensity columns is reduced for thinner areas of the sample, suggesting that $SrRuO_3$ surface steps (in the beam direction), rather than uniform intermixing, are the likely cause of the intermediate column intensities. With that in mind, we have chosen a thin sample area for our quantitative examination, where the results would not be affected by vertical averaging of different atom types. The interface was also analyzed by EELS. The profiles of La and Mn across the interface, together with HAADF intensity trace, are shown in Fig. 1(b). Note that (a) the La EELS signal extends beyond the Mn signal at the interface, indicating effective (La,Sr)O/RuO_2 termination and (b) the widths of the two EELS profiles are identical, indicating no or equivalent intermixing between both cationic sublattices.

The details of the interface structure were investigated by direct atomic position mapping.[11,13] Atomic positions were quantified directly from images using iterative center-of-mass algorithm; spacings were calibrated on the $SrTiO_3$ substrate. Typical maps of *c* lattice parameter (normal to the interface) are shown in Fig. 1(c). The *c*-parameter map shows that saturation lattice parameter decreases in $La_{0.7}Sr_{0.3}MnO_3$, in agreement

with the difference in bulk lattice parameters. It also shows some anomalies at the interface, as can be more clearly seen from the averaged profile in Fig. 1(d). The ∼1 unit cell (uc) thick layer of $SrRuO_3$ is slightly compressed approaching the interface, whereas the $La_{0.7}Sr_{0.3}MnO_3$ component shows expansion over ∼3 uc. To verify the statistical significance of the data, we used pairwise ANOVA comparisons at the 0.05 level of the columns in the map on Fig. 1(c). The data points for columns with the averages that are not significantly different from their neighbors are covered by the cross-hatched rectangles in Fig. 1(d).

The corresponding map and profile of a lattice parameters (parallel to the interface) are shown in Figs. 1(e) and 1(f). While the average a parameter is constrained to the same value on both sides of the interface by epitaxy, the lattice parameter map in the $SrRuO_3$ shows clear checkerboard pattern, indicative of the orthorhombic rather than cubic phase. This observation is in agreement with recent studies by the Eom group.[30] This orthorhombic distortion is, however, not expected to significantly affect the electronic and magnetic structure of $SrRuO_3$.[31] Note that the checkerboard pattern is nonuniform along the interface, and nominally cubic regions can penetrate by 3 to 4 uc in the $SrRuO_3$ layer, indicating a complex strain-related behavior. This modulation, while significant, is allowed by symmetry in the larger distorted $SrRuO_3$ unit cell and thus will not produce extra reflections in an x-ray diffraction study.

To complement lattice spacing maps, we show a cation displacement map in which displacements are calculated as the distance between the midpoint of the two adjacent Sr/La sublattice columns and the corresponding Ru/Mn column. The X (perpendicular to the interface) and Y (parallel to the interface) components of displacement are shown in Figs. 2(a) and 2(b); the averaged profile of the X displacement is shown in Fig. 2(c). In-plane displacement (Y) is near zero and shows a small change on transition to $La_{0.7}Sr_{0.3}MnO_3$, possibly due to a small relative misrotation of the $La_{0.7}Sr_{0.3}MnO_3$ and $SrRuO_3$ blocks. At the same time, the X displacement map shows an anomaly at the interface, with negative displacement in the $SrRuO_3$ region extending ∼3 uc inside the material, and positive displacement in the $La_{0.7}Sr_{0.3}MnO_3$ region extending ∼6. uc into the material (here, again we use cross-hatched rectangles to indicate the data points with displacement averages not significantly different from zero via ANOVA comparison at the 0.05 level); in our sign convention, both displacements constitute motion toward the interface. This behavior is highly unusual, given that both materials are nominally in the metallic state ($SrRuO_3$ is a majority electron metal; $La_{0.7}Sr_{0.3}MnO_3$ is a majority hole semimetal), and suggests the presence of built-in electric field at the $SrRuO_3$–$La_{0.7}Sr_{0.3}MnO_3$ junction.

To estimate the potential distribution in the vicinity of the interface, we adopt a phenomenological ansatz and assume that the displaced B cations (Mn and Ru) carry a nominal positive charge q_α, where $\alpha = 1, 2$ for the two sides of the interface. As in Refs. 24 and 26, we write the resulting polarization field on the two sides as

$$P_\alpha(z) = q_\alpha u_\alpha(z)/V_\alpha \tag{1}$$

where V_α are unit cell volumes, $u_\alpha(z)$ are the relative displacements of the B cations (see Fig. 2), and z is the distance across the interface (with the interface at $z = 0$). To determine the interfacial fields and potentials, we treat $P_\alpha(z)$ as a continuous function, which is in effect an interpolation of the original discrete dataset. To avoid artifacts from numerical differentiation of noisy input, we model $P_\alpha(z)$ by assuming that it arises from an effective charge density $\rho_\alpha^f(z)$, which we express as a sum of a finite number of step functions, $\rho_\alpha^f(z) = \sum_i \rho_{\alpha i}\theta(|z| - z_{\alpha i})\theta(z_{\alpha i} + W_{\alpha i} - |z|)$. The electrostatic potential $\varphi_\alpha(z)$ on each side of the interface is given by $\varepsilon_0\varepsilon_\alpha \partial^2\varphi_\alpha(z)/\partial z^2 = -\rho_\alpha^f(z)$, where ε_α are (bare) lattice permittivities. While $SrRuO_3$ and $La_{0.7}Sr_{0.3}MnO_3$ are metal and semimetal, respectively, the two materials can be treated as semiconductors for the purpose of this derivation.[32] The values of the lattice permittivities were taken from taken from Refs. 33 and 34 for $SrRuO_3$ and extrapolated for $La_{0.7}Sr_{0.3}MnO_3$ from the values for $LaMnO_3$ and $SrMnO_3$.[35] We enforce interfacial boundary conditions $\varphi(+0) = \varphi(-0) = U_b$ and $\varepsilon_0\varepsilon_1 E(-0) - \varepsilon_0\varepsilon_2 E(+0) = 0$, where $E(z) = -\partial\varphi(z)/\partial z$ and U_b are the difference in electron affinities in the two materials.

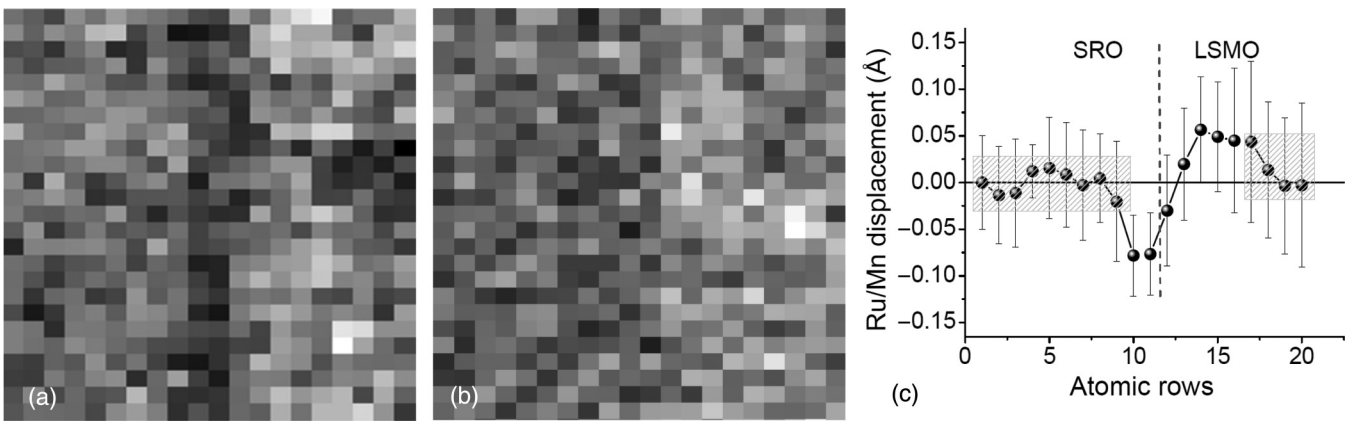

FIG. 2. (a) and (b) 2D maps of the (a) out-of-plane, or X and (b) in-plane, or Y Mn/Ru cation displacements computed from Fig. 1(a). (c) Profile of the map in (a) calculated by averaging along the interface. In Fig. 2(c), cross-hatched rectangles cover the points that do not show statistically significant changes (see text). Error bars in profile (c) show standard deviation with respect to averaging along the interface in the map (a).

The polarization field $P_\alpha(z)$ on the two sides is then given by $P_\alpha(z) = \varepsilon_0(\varepsilon_\alpha - 1)E_\alpha(z)$. In this way, $P_\alpha(z)$ is a function of the $\rho_{\alpha i}$. We then treat the $\rho_{\alpha i}$, $W_{\alpha i}$, and $z_{\alpha i}$ as free parameters and determine the best fit of the function $P_\alpha(z)$ to the discrete values given by the experimental data through Eq. (1). This procedure gives us the optimized functions $P_\alpha(z)$, $E_\alpha(z)$, and $\varphi_\alpha(z)$. To quantify the results, we adopted Bader charges for the q_α (calculated as 1.67 and 1.62 for Ru and Mn, respectively, as in Ref. 36). The results, with an overlay of recalculated experimental data, are plotted in Figs. 3(a)–3(c). Since the profiles showed very weak dependence on the interface potential difference U_b, it was set to zero. We note that the electrostatic potential in Fig. 3(c) has a pronounced dipolar character.

While the potential profile in Fig. 3(c) is quite wide, the related cation displacements are localized at the interface. Broadly speaking, the displacement of both Ru ions in $SrRuO_3$ and Mn ions in $La_{0.7}Sr_{0.3}MnO_3$ toward the interface implies electron doping by either free electrons or localized oxygen vacancies. To elucidate the atomic configuration most consistent with the observed cation displacements and dipolar character of the interface, we conducted a DFT study. Calculations were performed within the framework of the plane-wave basis set and projector-augmented-wave method implemented in the Vienna *Ab initio* Simulation Package (VASP).[37,38] The spin-polarized generalized-gradient approximation is applied to the ground state structures of $La_{0.7}Sr_{0.3}MnO_3$ (rhombohedral, space group $R\bar{3}c$) and $SrRuO_3$ (orthorhombic, space group *Pnma*). The Sr doping is considered by the substitution of Sr at La sites with a ratio of 1:3, and the magnetic states are relaxed in collinear configurations. Through structure relaxation, the magnetic coupling at $La_{0.7}Sr_{0.3}MnO_3$–$SrRuO_3$ interfaces on a $SrTiO_3$ substrate is found to be antiferromagnetic, which is in agreement with a previous DFT study.[28]

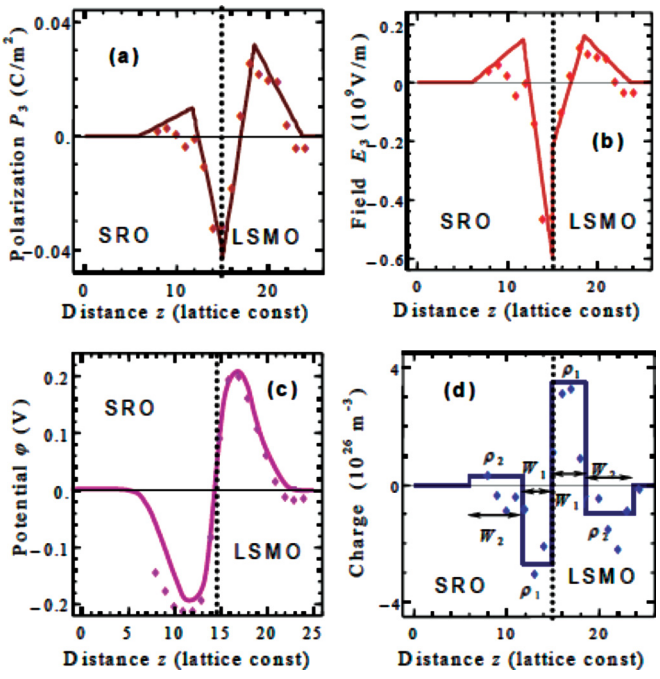

FIG. 3. (Color online) Polarization (a), electric field (b), potential (c), and effective charge density (d) profiles reconstructed from experimental atomic displacement data. Filled symbols in (a)–(d) are calculated from experimental atomic displacement data [Fig. 1(c)]. Solid curves are calculated self-consistently for material parameters in text.

To consider intrinsic free-electron doping at the interface (an effect often considered for oxide heterostructures such as $LaAlO_3/SrTiO_3$[39]), we first constructed interface models by joining stoichiometric $La_{0.7}Sr_{0.3}MnO_3$ and $SrRuO_3$ with the experimentally observed RuO_2/La(Sr)O termination. In this case, the La ions near the interface donate electrons to the interface and the interface is therefore doped by free electrons. However, the calculated B-site displacements with RuO_2/La(Sr)O termination are relatively small compared to the experimental data [Fig. 4(a), black squares], which is to be expected given that both $La_{0.7}Sr_{0.3}MnO_3$ and $SrRuO_3$ are nominally metallic (unlike $SrTiO_3$ or $LaAlO_3$), and thus capable of effectively screening interface charge with mobile charge carriers. Thus, the observed B-site polar displacements cannot be ascribed to chemical bonding effects and cation mismatch at the interface.

Based on the fact that no changes in composition and connectivity of the cation sublattice are visible by STEM, this leaves oxygen vacancy segregation as a possible source of the observed phenomena. To explore this possibility, DFT calculations were performed for multiple vacancy distribution scenarios. The results show that introducing even a single oxygen vacancy into the $La_{0.7}Sr_{0.3}MnO_3$ model near the interface leads to significant cation displacement [Fig. 4(a), red (dark gray) squares]; the shape of the profile becomes similar to the experimental data [see Fig. 2(c)], indicating qualitative agreement. When two oxygen vacancies are introduced into the near-interface region of $La_{0.7}Sr_{0.3}MnO_3$ [Fig. 4(a), blue (medium gray) squares], the overall shape of the profile is preserved, while the difference between the two extreme displacements (~0.11 Å) becomes comparable with the experimentally observed value of 0.12 Å (this concentration of vacancies corresponds to one quarter of a monolayer areal coverage of the interface plane). Note that when we introduce oxygen vacancies into the near-interface region of $SrRuO_3$, the resulting cation displacements are much smaller (not shown). Finally, we also considered different possible vacancy sites in $La_{0.7}Sr_{0.3}MnO_3$. When the vacancies are moved away from the interface, the displacements become much smaller, suggesting that the experimentally observed B-site polar displacement likely originates from the electron redistribution following introduction of multiple strongly localized oxygen vacancies in the $La_{0.7}Sr_{0.3}MnO_3$ near the $La_{0.7}Sr_{0.3}MnO_3$–$SrRuO_3$ interfaces. Thus, the structure model shown in Fig. 4(b) provides the best agreement with the experimental data.

Using these results, we evaluate the potential jump across the $La_{0.7}Sr_{0.3}MnO_3$–$SrRuO_3$ interface by calculating the electrostatic potentials experienced by the electrons in both the perfect $La_{0.7}Sr_{0.3}MnO_3$–$SrRuO_3$ supercell model and the model with two oxygen vacancies. To generate profiles across the interface, we performed macroscopic planar averaging of the DFT electrostatic potential along the z direction, followed by a sliding-window averaging of the difference between these two planar-averaged electrostatic potentials (no vacancies and two vacancies). The averaging window used was double the average lattice constants of these oxides. The resulting profile

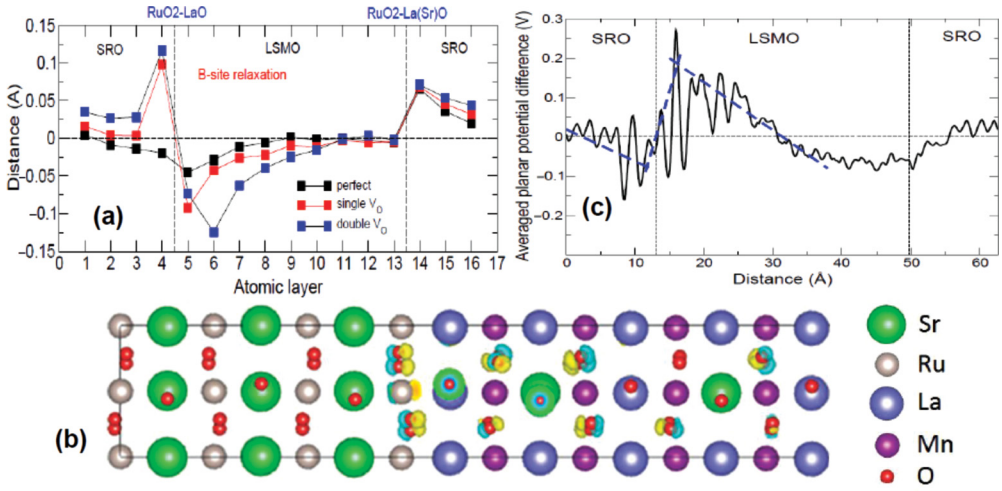

FIG. 4. (Color online) (a) Mn/Ru cation displacement profiles generated from density functional calculations for (La,Sr)O-RuO_2-terminated surface: free-electron doped (black squares), with one oxygen vacancy on the $La_{0.7}Sr_{0.3}MnO_3$ side [red (dark gray) squares], and with two oxygen vacancies on the $La_{0.7}Sr_{0.3}MnO_3$ side [blue (medium gray) squares]. (b) View of the interface in the structure model with two oxygen vacancies [denoted by red (dark gray) circles] showing the best agreement with the experiment; blue (medium gray) and yellow (light gray) lobes next to oxygen atoms show increase and decrease, respectively, in the electron density compared to the model without vacancies. (c) The difference between planar averaged electric potentials for the case with two vacancies [model in Fig. 4(b)] vs no vacancies.

is given in Fig. 4(c); note the characteristic dipolar shape. Notably, to compare this figure to Fig. 3(c), one needs to multiply it by -1, as Fig. 4(c) gives a potential experienced by an electron, while Fig. 3(c) gives a potential experienced by e unit positive charge. Note that both the magnitude and spatial localization of electric fields reconstructed from STEM data in Fig. 3(c) and from DFT are quite close; the full numerical equivalence cannot be expected given that the estimate in Fig. 3(c) did not take the contribution of oxygen anion displacements into account (however, as the DFT calculations show, the O displacements are largely rotations). We also note that the finding that oxygen vacancies are causing the observed displacements does not invalidate the phenomenological model that we employed to describe the macroscopic polarization and potential at the interfaces, since the vacancies cause the effective electric field that displaces the cations. Thus, we can conclude that direct image analysis of the STEM data allows us to obtain polarization and electric fields in the material.

We further note that a large concentration of oxygen vacancies could have produced a measurable change in EELS spectra, either in the integrated signal of the O *K* edge or in its fine structure. However, on transition from $La_{0.7}Sr_{0.3}MnO_3$ to $SrRuO_3$ both the integrated O *K* signal and the "pre-peak" intensity undergo significant changes (∼50% total) due to differences in metal-oxygen orbital coupling for Mn (3d) and Ru (4d), thus effectively masking any interface-specific contributions. At the same time, much more sensitive atomic displacement mapping allows us to uncover the underlying behavior quantitatively.

To summarize, we explored the atomic structure of the $SrRuO_3$–$La_{0.7}Sr_{0.3}MnO_3$ interface using direct structural imaging by STEM. This approach allows us to analyze the behavior at the $SrRuO_3$–$La_{0.7}Sr_{0.3}MnO_3$ interface, complementing recent work (Ref. 28), in which magnetic coupling was studied and ascribed predominantly to Mn/Ru intermixing. We attribute the observed phenomena to oxygen vacancy segregation at the interface, as suggested by the excellent agreement between the STEM data and DFT modeling. We further obtain quantitative agreement between electrostatic fields reconstructed from STEM data and from DFT. Beyond the $La_{0.7}Sr_{0.3}MnO_3$–$SrRuO_3$ system studied here, we note that this structural analysis can be extended to other oxide interfaces (as it has already been demonstrated for ferroelectrics[11,13,23–26,40]), complementing the traditional EELS imaging studies and providing secondary structural parameters of charge transfer, ionic effects, and order parameter couplings across correlated oxide interfaces.

The research is sponsored by the Division of Materials Sciences and Engineering, Office of Basic Energy Sciences, U.S. Department of Energy (A.Y.B., J.H., S.T.P., A.R.L., and S.J.P.). Research at Berkeley was sponsored by the SRC NRI-WIN program. Y.H.C. acknowledges the support of the National Science Council, R.O.C., under Contract No. NSC 100-2119-M-009-003.

*Corresponding author: albinab@ornl.gov

[1]N. Reyren, S. Thiel, A. D. Caviglia, L. Fitting Kourkoutis, G. Hammerl, C. Richter, C. W. Schneider, T. Kopp, A. S. Rüetschi, D. Jaccard, M. Gabay, D. A. Muller, J. M. Triscone, and J. Mannhart, Science **317**, 1196 (2007).

[2]A. Ohtomo and H. Y. Hwang, Nature (London) **427**, 423 (2004).

[3]S. M. Wu, Shane A. Cybart, P. Yu, M. D. Rossell, J. X. Zhang, R. Ramesh, and R. C. Dynes, Nat. Mater. **9**, 756 (2010).

[4]G. Gerra, A. K. Tagantsev, N. Setter, and K. Parlinski, Phys. Rev. Lett. **96**, 107603 (2006).

[5]M. Izumi, Y. Ogimoto, Y. Konishi, T. Manako, M. Kawasaki, and Y. Tokura, Mater. Sci. Eng. B **84**, 53 (2001).
[6]J. Chakhalian, J. W. Freeland, G. Srajer, J. Strempfer, G. Khaliullin, J. C. Cezar, T. Charlton, R. Dalgliesh, C. Bernhard, G. Cristiani, H. U. Habermeier, and B. Keimer, Nat. Phys. **2**, 244 (2006).
[7]J. Hoppler, J. Stahn, Ch Niedermayer, V. K. Malik, H. Bouyanfif, A. J. Drew, M. Roessle, A. Buzdin, G. Cristiani, H. U. Habermeier, B. Keimer, and C. Bernhard, Nat. Mater. **8**, 315 (2009).
[8]K. S. Takahashi, M. Kawasaki, and Y. Tokura, Appl. Phys. Lett. **79**, 1324 (2001).
[9]K. Ueda, H. Tabata, and T. Kawai, Science **280**, 1064 (1998).
[10]P. Yu, J. S. Lee, S. Okamoto, M. D. Rossell, M. Huijben, C. H. Yang, Q. He, J. X. Zhang, S. Y. Yang, M. J. Lee, Q. M. Ramasse, R. Erni, Y. H. Chu, D. A. Arena, C. C. Kao, L. W. Martin, and R. Ramesh, Phys. Rev. Lett. **105**, 027201 (2010).
[11]M. F. Chisholm, W. D. Luo, M. P. Oxley, S. T. Pantelides, and H. N. Lee, Phys. Rev. Lett. **105**, 197602 (2010).
[12]S. Saraf, M. Markovich, and A. Rothschild, Phys. Rev. B **82**, 245208 (2010).
[13]A. Y. Borisevich, H. J. Chang, M. Huijben, M. P. Oxley, S. Okamoto, M. K. Niranjan, J. D. Burton, E. Y. Tsymbal, Y. H. Chu, P. Yu, R. Ramesh, S. V. Kalinin, and S. J. Pennycook, Phys. Rev. Lett. **105**, 087204 (2010).
[14]S. J. May, J. W. Kim, J. M. Rondinelli, E. Karapetrova, N. A. Spaldin, A. Bhattacharya, and P. J. Ryan, Phys. Rev. B **82**, 014110 (2010).
[15]S. A. Chambers, M. H. Engelhard, V. Shutthanandan, Z. Zhu, T. C. Droubay, L. Qiao, P. V. Sushko, T. Feng, H. D. Lee, T. Gustafsson, E. Garfunkel, A. B. Shah, J. M. Zuo, and Q. M. Ramasse, Surf. Sci. Rep. **65**, 317 (2010).
[16]P. Zubko, S. Gariglio, M. Gabay, P. Ghosez, and J.-M. Triscone, Annu. Rev. Condens. Matter Phys. **2**, 141 (2011).
[17]J. F. Mitchell, D. N. Argyriou, C. D. Potter, D. G. Hinks, J. D. Jorgensen, and S. D. Bader, Phys. Rev. B **54**, 6172 (1996).
[18]W. Jiang, M. Noman, Y. M. Lu, J. A. Bain, P. A. Salvador, and M. Skowronski, J. Appl. Phys. **110**, 034509 (2011).
[19]H. T. Yi, T. Choi, S. G. Choi, Y. S. Oh, and S. W. Cheong, Adv. Mater. **23**, 3403 (2011).
[20]J. Gazquez, W. D. Luo, M. P. Oxley, M. Prange, M. A. Torija, M. Sharma, C. Leighton, S. T. Pantelides, S. J. Pennycook, and M. Varela, Nano Lett. **11**, 973 (2011).
[21]Y.-M. Kim, J. He, M. D. Biegalski, H. Ambaye, V. Lauter, H. M. Christen, S. T. Pantelides, S. J. Pennycook, S. V. Kalinin, and A. Y. Borisevich, Nat. Mater. **11**, 888 (2012).
[22]D. Tang, W. Z. Zhou, and J. M. Thomas, Angew. Chem., Int. Ed. Engl. **26**, 1048 (1987).
[23]C. L. Jia, S. B. Mi, K. Urban, I. Vrejoiu, M. Alexe, and D. Hesse, Nat. Mater. **7**, 57 (2008).
[24]C. L. Jia, V. Nagarajan, J. Q. He, L. Houben, T. Zhao, R. Ramesh, K. Urban, and R. Waser, Nat. Mater. **6**, 64 (2007).
[25]C. L. Jia, S. B. Mi, K. Urban, I. Vrejoiu, M. Alexe, and D. Hesse, Phys. Rev. Lett. **102**, 117601 (2009).
[26]C. T. Nelson, B. Winchester, Y. Zhang, S. J. Kim, A. Melville, C. Adamo, C. M. Folkman, S. H. Baek, C. B. Eom, D. G. Schlom, L. Q. Chen, and X. Q. Pan, Nano Lett. **11**, 828 (2011).
[27]S. J. Pennycook and P. D. Nellist, *Scanning Transmission Electron Microscopy* (Springer, New York, 2011).
[28]M. Ziese, I. Vrejoiu, E. Pippel, P. Esquinazi, D. Hesse, C. Etz, J. Henk, A. Ernst, I. V. Maznichenko, W. Hergert, and I. Mertig, Phys. Rev. Lett. **104**, 167203 (2010).
[29]L. Fitting Kourkoutis, J. H. Song, H. Y. Hwang, and D. A. Muller, Proc. Natl. Acad. Sci. USA **107**, 11682 (2010).
[30]K. J. Choi, S. H. Baek, H. W. Jang, L. J. Belenky, M. Lyubchenko, and C.-B. Eom, Adv. Mater. **22**, 759 (2009).
[31]J. M. Rondinelli, N. M. Caffrey, S. Sanvito, and N. A. Spaldin, Phys. Rev. B **78**, 155107 (2008).
[32]R. R. Mehta, B. D. Silverma, and J. T. Jacobs, J. Appl. Phys. **44**, 3379 (1973).
[33]D. J. Kim, J. Y. Jo, Y. S. Kim, Y. J. Chang, J. S. Lee, J. G. Yoon, T. K. Song, and T. W. Noh, Phys. Rev. Lett. **95**, 237602 (2005).
[34]W. Siemons, G. Koster, A. Vailionis, H. Yamamoto, D. H. A. Blank, and M. R. Beasley, Phys. Rev. B **76**, 075126 (2007).
[35]J. L. Cohn, M. Peterca, and J. J. Neumeier, Phys. Rev. B **70**, 214433 (2004).
[36]W. Tang, E. Sanville, and G. Henkelman, J. Phys.: Condens. Matter **21**, 084204 (2009).
[37]W. Kohn and L. J. Sham, Phys. Rev. **140**, 1133 (1965).
[38]G. Kresse and J. Furthmüller, Phys. Rev. B **54**, 11169 (1996).
[39]G. Herranz, M. Basletic, M. Bibes, C. Carretero, E. Tafra, E. Jacquet, K. Bouzehouane, C. Deranlot, A. Hamzic, J. M. Broto, A. Barthelemy, and A. Fert, Phys. Rev. Lett. **98**, 216803 (2007).
[40]H. J. Chang, S. V. Kalinin, A. N. Morozovska, M. Huijben, Y. H. Chu, P. Yu, R. Ramesh, E. A. Eliseev, G. S. Svechnikov, S. J. Pennycook, and A. Y. Borisevich, Adv. Mater. **23**, 2474 (2011).